J|A|C|S
ARTICLES
Published on Web 01/05/2006

A Three-State Mechanism for DNA Hairpin Folding Characterized by Multiparameter Fluorescence Fluctuation Spectroscopy

Jaemyeong Jung and Alan Van Orden*

Contribution from the Department of Chemistry, Colorado State University, Fort Collins, Colorado 80523

Received September 2, 2005; E-mail: vanorden@lamar.colostate.edu

Abstract: The folding of a dye-quencher labeled DNA hairpin molecule was investigated using fluorescence autocorrelation and cross-correlation spectroscopy (FCS) and photon counting histogram analysis (PCH). The autocorrelation and cross-correlation measurements revealed the flow and diffusion times of the DNA molecules through two spatially offset detection volumes, the relaxation time of the folding reaction, and the total concentration of DNA molecules participating in the reaction. The PCH measurements revealed the equilibrium distribution of DNA molecules in folded and unfolded conformations and the specific brightnesses of the fluorophore in each conformational state. These measurements were carried out over a range of NaCl concentrations, from those that favored the open form of the DNA hairpin to those that favored the closed form. DNA melting curves obtained from each sample were also analyzed for comparison. It was found that the reactant concentrations were depleted as the reaction progressed and that the equilibrium distributions measured by FCS and PCH deviated from those obtained from the melting curve analyses. These observations suggest a three-state mechanism for the DNA hairpin folding reaction that involves a stable intermediate form of the DNA hairpin. The reaction being probed by FCS and PCH is suggested to be a rapid equilibrium between open and intermediate conformations. Formation of the fully closed DNA hairpin is suggested to occur on a much longer time scale than the FCS and PCH measurement time. The closed form of the hairpin thus serves as a sink into which the reactants are depleted as the reaction progresses.

Introduction

DNA stem-loop hairpins are model systems for secondary structure formation in single-stranded DNA and RNA.[1−5] In recent years, there has been a resurgence of interest relating to the kinetics and energetics of DNA hairpin folding, fueled in part by new experimental techniques for probing the microsecond time scale on which these reactions occur.[6−16] These experiments include laser-induced temperature jump spectroscopy[6,9,11,16] and fluorescence correlation spectroscopy (FCS).[7,8,12−15] Chemical relaxation processes attributed to DNA hairpin folding and unfolding are routinely observed. Relaxation times depend on the size of the hairpin loop, the number of base pairs in the stem, and the loop sequence and can range from a few microseconds to hundreds of microseconds. It has generally been assumed that these relaxation processes describe a predominantly two-state reaction in which the DNA molecules spend most of their time in a fully folded stem-loop hairpin structure or a fully unfolded random coil configuration. Partially folded or misfolded intermediates are thought to exist as transient traps in the overall folding reaction.[7,9,17]

In a previous study, we characterized the relaxation times of DNA hairpin folding reactions using a new "multiparameter" approach to FCS.[15] This technique analyzes the fluorescence observed from a flowing sample of DNA hairpin molecules at two spatially offset detection volumes. Simultaneous cross-correlation and autocorrelation analysis of the fluorescence from the two detection volumes resolves the transport properties of the molecules from their chemical relaxation properties and,

(1) Cantor, C. R.; Schimmel, P. R. *Biophysical Chemistry: the Behavior of Biological Macromolecules*; Freeman: New York, 1980.
(2) Tyagi, S.; Kramer, F. R. *Nat. Biotechnol.* **1996**, *14*, 303−308.
(3) Bonnet, G.; Tyagi, S.; Libchaber, A.; Kramer, F. R. *Proc. Natl. Acad. Sci. U.S.A.* **1999**, *96*, 6171−6176.
(4) Liu, X.; Tan, W. *Anal. Chem.* **1999**, *71*, 5054−5059.
(5) Wang, X.; Nau, W. M. *J. Am. Chem. Soc.* **2004**, *126*, 808−813.
(6) Ansari, A.; kuznetosov, S. V.; Shen, Y. *Proc. Natl. Acad. Sci. U.S.A.* **2001**, 98, 7771−7776.
(7) Bonnet, G.; Krichevsky, O.; Libchaber, A. *Proc. Natl. Acad. Sci. U.S.A.* **1998**, *95*, 8602−8606.
(8) Goddard, N. L.; Bonnet, G.; Krichevsky, O.; Libchaber, A. *Phys. Rev. Lett.* **2000**, *85*, 2400−2403.
(9) Kuznetosov, S. V.; Shen, Y.; Benight, A. S.; Ansari, A. *Biophys. J.* **2001**, *81*, 2864−2875.
(10) Senior, M. M.; Jones, R. A.; Breslauer, K. J. *Proc. Natl. Acad. Sci. U.S.A.* **1988**, *85*, 6242−6246.
(11) Shen, Y.; kuznetosov, S. V.; Ansari, A. *J. Phys. Chem. B* **2001**, *105*, 12202−12211.
(12) Wallace, M. I.; Ying, L.; Balasubramanian, S.; Klenerman, D. *J. Phys. Chem. B* **2000**, *104*, 11551−11555.
(13) Wallace, M. I.; Ying, L.; Balasubramanian, S.; Klenerman, D. *Proc. Natl. Acad. Sci. U.S.A.* **2001**, *98*, 5584−5589.
(14) Li, H.; Ren, H.; Ying, L.; Balasubramanian, S.; Klenerman, D. *Proc. Natl. Acad. Sci. U.S.A.* **2004**, *101*, 14425−14430.
(15) Jung, J.; Van Orden, A. *J. Phys. Chem. B* **2005**, *109*, 3648−3657.
(16) Ansari, A.; Kuznetosov, S. V. *J. Phys. Chem. B* **2005**, *109*, 12982−12989.
(17) Ying, L.; Wallace, M. I.; Klenerman, D. *Chem. Phys. Lett.* **2001**, *334*, 145−150.

10.1021/ja0560736 CCC: $33.50

thus, allows more information to be drawn from the system than could be obtained using conventional single-beam FCS alone.

The present study combines this multiparameter FCS technique with photon counting histogram (PCH) analysis,[18−20] which monitors the absolute and relative concentrations of the reactants taking part in the observed chemical relaxation process, in addition to the reaction time. We studied the folding of a stem-loop DNA hairpin molecule containing five base pairs in the stem and twenty-one thymine residues in the loop region. The reaction conditions were varied from those favoring the open form of the DNA hairpin to those favoring the closed form. Our results do not support a predominantly two-state reaction mechanism for the folding of this DNA hairpin, as has previously been thought. For example, one of our key observations is that the overall reactant concentration was dramatically depleted as the reaction conditions were altered in favor of the closed form of the hairpin. This observation cannot be explained from the standpoint of a two-state reaction mechanism. If only two states were present, the relative concentrations of the reactants would change, but the overall reactant concentration would stay constant. We can explain this and other observations presented below by assuming the chemical relaxation process being probed by FCS and PCH involves an intermediate form of the DNA hairpin that is stable on the time scale of the observed reaction. The fully folded configuration is not directly observed in our FCS and PCH measurements but is observed indirectly as a stable sink into which the reactants become transformed as the reaction progresses. Our observations suggest a three-state DNA hairpin folding mechanism involving a rapid equilibrium between open and intermediate configurations. The fully folded DNA hairpin forms much more slowly and, once formed, is extremely stable on the time scale of our experiment. Hence, we describe a DNA hairpin folding reaction that is even more complex and more drawn out than previously thought.

Experimental Section

Details of the experiment were described previously.[15] Briefly, the DNA hairpins were dual-labeled with Rhodamine 6G (R6G) and 4-{[4-(dimethylamino)phenyl]axo}benzoic acid (dabcyl) at the 5′ and 3′ ends, respectively. The hairpin sequence was 5′-R6G-AACCC-$(T)_{21}$-GGGTT-dabcyl-3′. DNA solutions with nanomolar DNA concentrations were prepared in a pH ∼8.0 buffer solution containing 2.5 mM Tris-HCl, 250 μM EDTA, and various concentrations of NaCl.

The FCS and PCH experimental setup is shown in Figure 1. The sample solutions were flowed continuously through the capillary by pressurizing the capillary inlet with N_2 gas. Fluorescence fluctuation spectroscopy (FFS) measurements were performed using a home-built single molecule confocal fluorescence microscope.[21] Two split laser beams (514.5 nm, 40 μW per beam before focus lens) were focused into the capillary by a 100× 1.25 NA oil immersion microscope objective. Fluorescence from each focal region was collected through the same objective; passed through the 530 nm long pass dichroic mirror; split by 50/50 beam splitter; and then imaged into two 50 μm confocal pinholes separately, (Thorlabs, Newton, NJ) which provide axial resolution by rejecting out-of-focus light. The output of the pinholes was band-pass filtered and focused onto the active areas of two single-photon-counting avalanche photodiode detectors. The two laser beams formed nearly identical diffraction-limited focal regions, positioned near the center of the inner capillary space (∼25-μm from the inner surfaces), separated along the axial dimension of the capillary by a distance of ∼2 to 3 μm. The optimum position of the two laser beam foci relative to the *z*-position of the capillary and the flow axis could be confirmed by cross-correlation analysis.[22,23] The entire experiment was placed inside an enclosure to block stray laser light. All experiments were carried out at an ambient temperature of ∼19 °C.

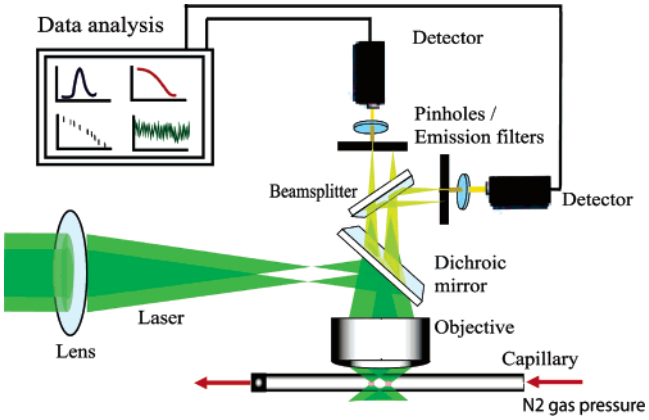

Figure 1. Schematic representation of the two-beam fluorescence fluctuation spectroscopy experiment. The optical setup was designed to position the two laser beams in the center of the squared capillary, separated by a distance of ∼2−3 μm. The sample solution flows through the capillary under applied gas pressure. Fluorescence signal from each laser focal volume is collected and used for the simultaneous analysis of autocorrelation and cross-correlation as well as PCH.

The photocounts from the two detectors were recorded using the two channels of a 800-MHz gated photon counter (PMS-400, Becker & Hickl GmbH, Berlin, Germany), interfaced to a Pentium computer. A sampling time of 1-μs per sampling interval was used for each channel. A LabView computer program, written in-house, was used to perform real-time FFS analysis on the detected photons as they were being accumulated. The program simultaneously autocorrelated the photocounts observed from the individual detection volumes and cross-correlated the photocounts from the two detection volumes relative to each other. The cross-correlation functions were calculated after first rebinning the accumulated photocounts into 9 μs sampling intervals to achieve improved signal-to-noise ratio. All correlation functions were calculated using the "multiple-τ" concept, in which the intervals between successive lagtimes increase as the lagtime increases. The rebinned photocounts of 9 μs sampling intervals were also used to construct photon counting histograms. The histograms obtained from each detection channel were identical within experimental error. The user interface of the LabView program continuously displays a running average of the correlation functions and the cumulative histograms. The experimental photon counting distribution $\{p_k\}$ was analyzed by fitting the normalized histogram to a theoretical PCH model,$\{\bar{p}_k\}$, devised by Perroud et al.[20] The PCH fitting quality is determined by estimating reduced χ^2_{red} based on a binomial distribution statistics.[18,24]

(18) Chen, Y.; Muller, J. D.; So, P.; Gratton, E. *Biophys. J.* **1999**, *77*, 553−567.
(19) Kask, P.; Palo, K.; Ullmann, D.; Gall, K. *Proc. Natl. Acad. Sci. U.S.A.* **1999**, *96*, 13756−13761.
(20) Perroud, T. D.; Huang, B.; Wallace, M. I.; Zare, R. N. *ChemPhysChem* **2003**, *4*, 1121−1123.
(21) Van Orden, A.; Fogarty, K.; Jung, J. *Appl. Spectrosc.* **2004**, *58*, 122A−137A.
(22) Brinkmeier, M.; Dorre, K.; Stephan, J.; Eigen, M. *Anal. Chem.* **1999**, *71*, 609−616.
(23) Gosch, M.; Blom, H.; Holm, J.; Heino, T.; Rigler, R. *Anal. Chem.* **2000**, *72*, 3260−3265.
(24) Huang, B.; Perroud, T. D.; Zare, R. N. *ChemPhysChem* **2004**, *5*, 1523−1531.

$$\chi^2_{\mathrm{red}} = \frac{\sum_{k_{\min}}^{k_{\max}} r_k^2}{k_{\max} - k_{\min} - d} \tag{1}$$

where, d is number of fitting parameters and r_k is a normalized residual given by

$$r_k = \frac{N(p_k - \bar{p}_k)}{\sigma_k} \tag{2}$$

where N is the total number of experimental data points in the histogram and σ_k is a standard deviation given by

$$\sigma_k = \sqrt{N p_k (1 - p_k)} \tag{3}$$

Analyses of both experimental correlation functions and photon counting distribution were carried out using a Levenberg−Marquardt algorithm (least-squares fitting routine) from the MatLab Optimization Toolbox.

Results and Discussion

FCS and PCH Analysis. We begin by describing our efforts to evaluate our FCS and PCH measurements assuming a DNA hairpin folding reaction that goes to completion via a two-state reaction process:

$$\bar{N}_1 \underset{k_{-1}}{\overset{k_1}{\rightleftharpoons}} \bar{N}_2 \tag{4}$$

Here, $\bar{N}_1$ and $\bar{N}_2$ refer to the average number of DNA hairpin molecules occupying the detection volume of the optical microscope in their open and closed conformations, respectively. Figure 2A displays autocorrelation and cross-correlation functions (inset) obtained from DNA hairpin samples containing constant DNA concentration and varying NaCl concentrations. The cross-correlation functions, $G_{C,2S}(\tau)$, were analyzed by fitting to eq 5:[22,23,25−29]

$$G_{C,2S}(\tau) - 1 = \frac{1}{\bar{N}_1 + \bar{N}_2}\left(\frac{1}{1 + \tau/\tau_D}\right)\left(\frac{1}{1 + \kappa_0^2 \tau/\tau_D}\right)^{1/2} \exp\left(-\frac{r^2(1 - \tau/\tau_F)^2}{1 + \tau/\tau_D}\right)$$

$$= \frac{1}{\bar{N}_{CC}} g_D(\tau) g_{Fc}(\tau) \tag{5}$$

where

$$g_D(\tau) = \left(\frac{1}{1 + \tau/\tau_D}\right)\left(\frac{1}{1 + \kappa_0^2 \tau/\tau_D}\right)^{1/2} \tag{6}$$

$$g_{Fc}(\tau) = \exp\left(-\frac{r^2(1 - \tau/\tau_F)}{1 + \tau/\tau_D}\right) \tag{7}$$

The parameter τ_D is the average diffusion time of the DNA molecules through the detection volume. κ_0 is the ratio (ω_0/z_0) of the radial, ω_0, and axial, z_0, focal radii and has been held constant at the value 0.104 ± 0.002 determined previously. r is the ratio (R/ω_0) of the distance, R, between the two detection volumes and the focal radius, ω_0. τ_F is the average flow time of the DNA molecules between the two focal volumes and is equal to R/V_x, where V_x is the linear flow velocity of the analyte solution at the point of detection. Finally, $\bar{N}_{CC}$ represents the average number of DNA hairpin molecules in both open and closed conformations occupying the detection volume ($\bar{N}_{CC} = \bar{N}_1 + \bar{N}_2$).

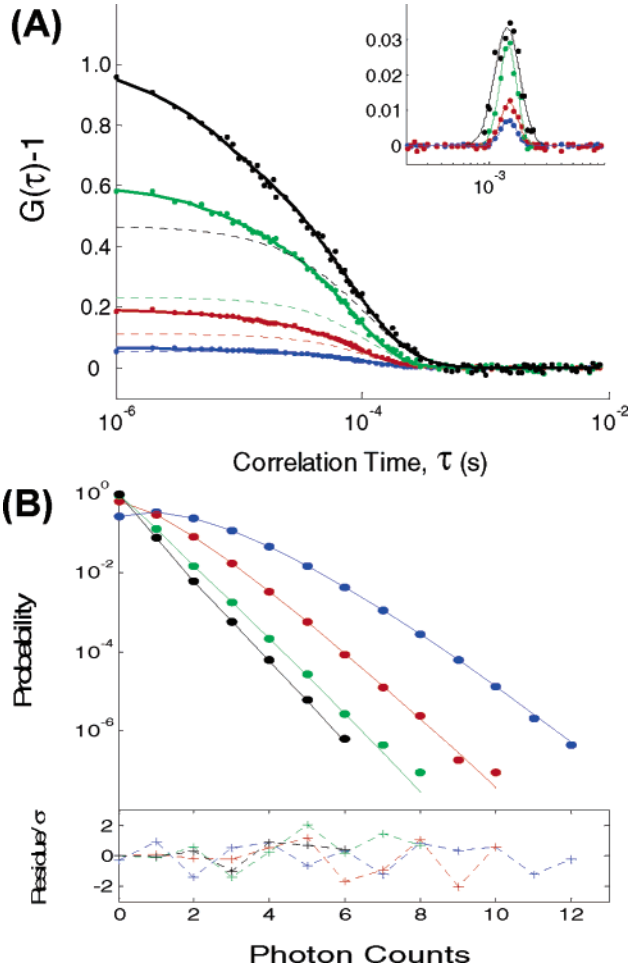

Figure 2. Experiment data (dots) and corresponding fitting curves (solid lines) from simultaneous FCS and PCH measurements vs NaCl concentration (blue, 0; green, 25; red, 100; and black, 500 mM NaCl). (A) The observed autocorrelation functions, with the cross-correlation functions shown in the inset. The dashed curves are the predicted autocorrelation functions assuming pure diffusion and flow. (B) The photon counting histograms obtained from the same samples using 9 μs sampling intervals. The DNA concentration was held constant at ~25 nM for all the samples.

For a two-state chemical reaction with a relaxation time faster than the flow time (τ_F), the cross-correlation function is only sensitive to the diffusion and flow properties of the DNA molecules.[15] Fluorescence fluctuations caused by the reaction are not sufficiently correlated with respect to the two detection volumes under these conditions. Cross-correlation analysis thus gives the parameters τ_D, τ_F, r, and $\bar{N}_{CC}$, without contributions from chemical relaxation. The dotted curves in Figure 2A predict how the autocorrelation functions would appear under conditions of pure diffusion and flow of the DNA molecules, based on the measured cross-correlation parameters. Any deviation between the predicted and observed autocorrelation functions is attributed to relaxation caused by triplet blinking at shorter time scales and quenching and unquenching of the fluorescent dye, induced by DNA conformational fluctuations, at longer time scales.

Table 1. Parameters form EFS Analysis[a,b]

PCH analysis[c]			FCS analysis			
	one	two				
model:	species	species	cross-correlation		autocorrelation	
$\bar{N}_{app}$	1.54(03)	1.44(55)	r	11.8(06)	T_{eq}	0.198(24)
ϵ_{app}	0.539(31)	0.48(19)	$\bar{N}_{cc}$	4.26(05)	B_{eq}	0.987(97)
			τ_F (ms)	1.47(15)	τ_T (μs)	4.12(71)
$\bar{N}_1$	1.27(12)	0.72(16)	τ_D (μs)	214(13)	τ_R (μs)	62.7(5.1)
$\bar{N}_2$	2.98(22)	0.98(25)				
ϵ_1	0.591(17)	0.61(14)			$[G(0) - 1]^{-1}$	1.65(01)
ϵ_2	0.074(14)	0.26(12)				
F	0.732(54)	0.71(16)				
χ^2	1.75	1.69				
K_{FFS}	2.33(22)	1.36(46)				
Q	0.125(24)	0.42(22)				

[a] Parameters correspond to the fitting analysis in Figure 1 (100 mM NaCl). [b] Values in parentheses are the standard deviation for the last digits. [c] Values underlined are calculated using fitting parameters.

Parameters relating to the chemical relaxation of the DNA hairpin structure were obtained by fitting the experimental autocorrelation functions to eq 8, which shows the theoretical autocorrelation function, $G_{A,2S}(\tau)$, describing two-state chemical relaxation.[25,30−36]

$$G_{A,2S}(\tau) - 1 = \frac{1}{\bar{N}_{CC}} g_D(\tau)(1 + T_{eq}e^{-\tau/\tau_T})[1 + B_{eq}e^{-\tau/\tau_R}] \times \exp\left(-\frac{(r\tau/\tau_F)^2}{1 + \tau/\tau_D}\right) = \frac{1}{\bar{N}_{CC}} g_D(\tau)g_T(\tau)g_R(\tau)g_{Fa}(\tau) \quad (8)$$

where

$$g_T(\tau) = \frac{1 - T + Te^{-\tau/\tau_T}}{1 - T} = 1 + T_{eq}e^{-\tau/\tau_T} \quad (9)$$

$$g_R(\tau) = \frac{1 - B + Be^{-\tau/\tau_R}}{1 - B} = 1 + B_{eq}e^{-\tau/\tau_R}, \text{ and} \quad (10)$$

$$g_{Fa}(\tau) = \exp\left(-\frac{(r\tau/\tau_F)^2}{1 + \tau/\tau_D}\right) \quad (11)$$

Here, T is the quantum yield, and τ_T is the time constant for triplet blinking; τ_R is the relaxation time of the two-state reaction; and B is an amplitude term that depends on the equilibrium distribution of the reactants and their specific brightnesses. These parameters were determined by constraining τ_D, τ_F, r, and $\bar{N}_{CC}$ to the values obtained in the cross-correlation analysis and adjusting τ_T, T_{eq}, τ_R, and B_{eq} to achieve the best fit. Representative results from our autocorrelation and cross-correlation analyses are presented in Table 1. Relaxation times

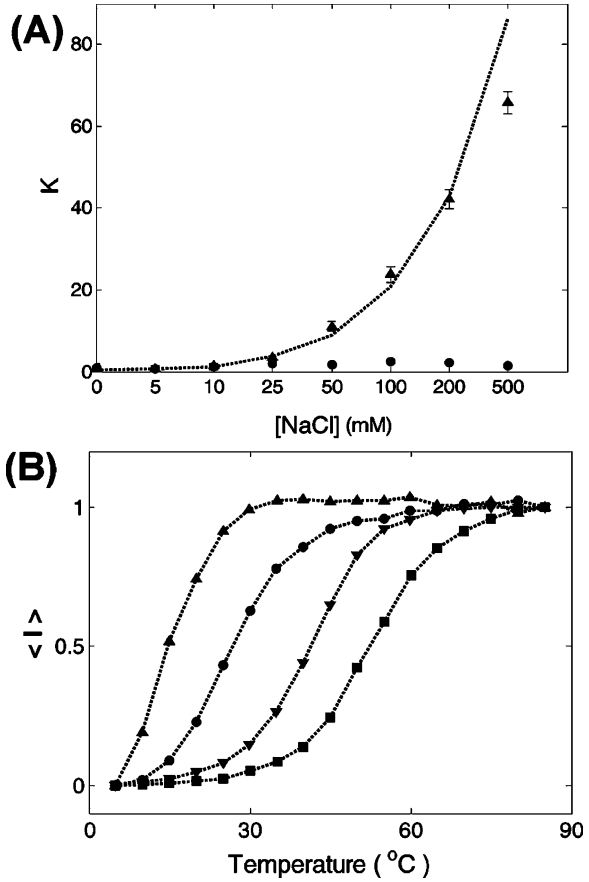

Figure 3. (A) Equilibrium constants of DNA hairpin samples vs NaCl concentration and (B) corresponding melting profiles [data sets with NaCl concentrations of 0 (▲), 25 (●), 100 (▼), and 500 mM (■) are shown]. In panel A, K_{melt} (▲) represents the equilibrium constants evaluated from the melting curves according to eq 12. K_{FFS} (●) represents the equilibrium constants determined from our FCS and PCH analysis. The dotted line in panel A is $K_{melt,3S}$ calculated according to eq 25.

(τ_R) for the DNA hairpin folding reaction were observed to be ~60 μs, consistent with previous kinetics experiments on the folding of DNA hairpins with the same size and composition as the one studied here.[7,8,15]

What is of interest to us here is the equilibrium distribution of folded and unfolded DNA hairpin molecules as a function of NaCl concentration. It is known that NaCl stabilizes the folded form of the hairpin.[37] This is evident from the melting curves displayed in Figure 3B, which show the characteristic rise in melting temperature with added NaCl. If a two-state reaction is assumed, the melting curves can be analyzed to determine the equilibrium constant $K_{melt} = \bar{N}_2/\bar{N}_1$ using eq 12:

$$K_{melt}(T) = \frac{I(85\,°C) - I(T)}{I(T) - I(5\,°C)} \quad (12)$$

where $I(T)$ is the fluorescence intensity at temperature T. We have evaluated K_{melt} for each sample at our laboratory temperature of 19 °C (See Figure 3A). As expected, K_{melt} rises precipitously with added NaCl.

Our initial goal was to simply characterize this behavior using our fluorescence fluctuation spectroscopy data itself, without reference to the DNA melting curves. The correlation amplitude

(25) Magde, D.; Webb, W. W.; Elson, E. L. *Biopolymers* **1978**, *17*, 361−376.
(26) Dittrich, P. S.; Schwille, P. *Anal. Chem.* **2002**, *74*, 4472−4479.
(27) Kunst, B. H.; Schots, A.; Visser, A. J. W. G. *Anal. Chem.* **2002**, *74*, 5350−5357.
(28) LeCaptain, D. J.; Van Orden, A. *Anal. Chem.* **2002**, *74*, 1171−1176.
(29) Fogarty, K.; Van Orden, A. *Anal. Chem.* **2003**, *75*, 6634−6641.
(30) Elson, E. L.; Magde, D. *Biopolymers* **1974**, *13*, 1−27.
(31) Magde, D.; Elson, E. L.; Webb, W. W. *Biopolymers* **1974**, 13, 29−61.
(32) Palmer, A. G.; Thompson, N. L. *Biophys. J.* **1987**, *51*, 339−343.
(33) Widerngren, J.; Mets, U.; Rigler, R. *J. Phys. Chem. B* **1995**, *99*, 13368−13379.
(34) Widerngren, J.; Rigler, R. *Cell. Mol. Biol.* **1998**, *44*, 857−879.
(35) Van Orden, A.; Keller, R. A. *Anal. Chem.* **1998**, *70*, 4463−4471.
(36) Rigler, R.; Eigen, E. L. *Fluorescence Correlation Spectroscopy: Theory and Applications*; Springer-Verlag: Berlin, 2001.
(37) Manning, G. S. *Q. Rev. Biophys.* **1978**, *11*, 179−246.

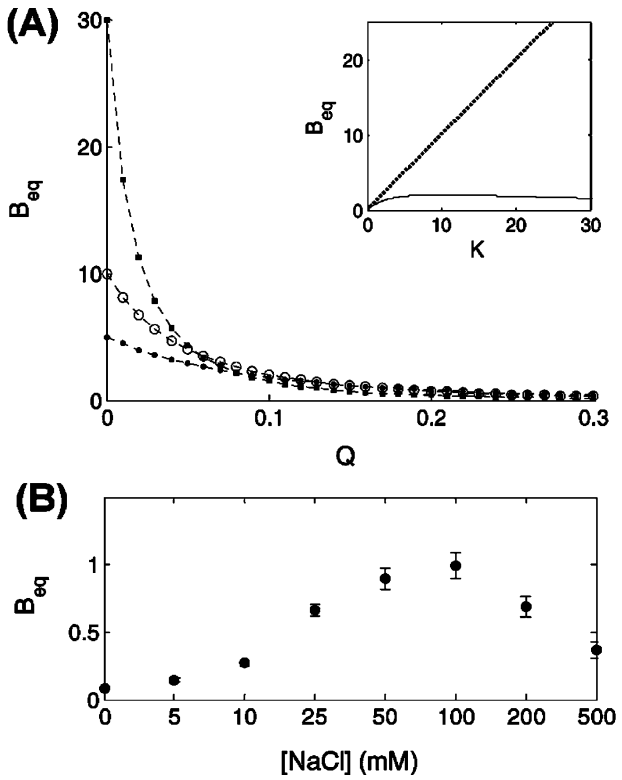

Figure 4. (A) Simulations of the amplitude term B_{eq} as function of Q and K (inset), and (B) experimental B_{eq} values from FCS analysis of DNA hairpin samples. Panel A shows three equilibrium constants (●) $K = 5$, (○) K = 10, (■) K = 30). Note that at $Q = 0$, $B_{eq} = K$. As Q deviates from 0, the values of B_{eq} become considerably different from K. For instance, the difference between cases of $Q = 0$ (dotted line) and $Q = 0.1$ (solid line) is shown in the inset. According to observed values in panel B, the expected Q is greater than ~0.1 in our experiments.

parameters $\bar{N}_{CC}$ and B_{eq} contain information about the reaction equilibrium. In particular, B_{eq} has the form:

$$B_{eq} = K_{FFS}\left[\frac{1-Q}{1+K_{FFS}Q}\right]^2 = \frac{\bar{N}_1\bar{N}_2(\epsilon_1-\epsilon_2)^2}{(\bar{N}_1\epsilon_1+\bar{N}_2\epsilon_2)^2} \qquad (13)$$

K_{FFS} denotes the equilibrium constant as determined by our fluctuation spectroscopy measurements; ϵ_1 and ϵ_2 are the specific brightnesses of R6G when the DNA hairpin molecules are in their open and closed conformations, respectively, and Q is the ratio ϵ_2/ϵ_1. The B_{eq} parameter is sometimes used to estimate K_{FFS} based on the assumption that $Q \approx 0$. However, this is often a very severe approximation that must be used with great care. As shown in Figure 4A, when $Q > \sim 0.1$, the measured value of B_{eq} can support a broad range of K_{FFS} values. B_{eq} essentially loses its dependence on K_{FFS} under these conditions. It is also seen that B_{eq} only takes on values greater than 1 when $Q \ll \sim 0.1$. Our B_{eq} measurements (Figure 4B) are in the regime where $B_{eq} < \sim 1$ and $Q > \sim 0.1$. This means that K_{FFS} and Q cannot be resolved using our FCS measurements alone. Additional information is needed to resolve these parameters.

Our motivation for combining PCH with FCS was to address this issue. The PCH is a probability distribution for detecting k photons arising from the optical detection volume during a specified sampling interval.[18,19] The probability depends on the average number of fluorescent molecules being probed by the optical microscope and their specific brightnesses. This is precisely the information needed to resolve the K_{FFS} and Q terms contained in the B_{eq} parameter. Figure 2B shows photon counting histograms obtained from the same DNA samples represented by the corresponding FCS data in Figure 2A. The 9 μs counting intervals were chosen to be small compared to the relaxation time of the DNA hairpin folding reaction, such that the system could be considered static on the time scale of the PCH measurement. Two approaches for obtaining the desired information from these data were investigated. To simplify matters, we note that ϵ_1 is the specific brightness of unquenched R6G, which we have measured separately by PCH analysis of R6G labeled DNA in the absence of quencher (See Supporting Information). The challenge becomes one of determining $\bar{N}_1$, $\bar{N}_2$, and ϵ_2.

The first PCH analysis approach we investigated was to determine $\bar{N}_1$, $\bar{N}_2$, and ϵ_2 directly by fitting the observed PCH to a two-species model of the probability distribution. The model we used was that of Perroud et al.[20] These authors devised a way to correct for the contribution to the PCH from out-of-focus emission due to one-photon fluorescence excitation. For a one-component system, the probability for detecting k photon counts from $\bar{N}$ identical molecules with a specific brightness, ϵ, is given by

$$P(k;\bar{N},\epsilon) = \sum_{N=0}^{\infty} p^{(N)}(k;q,\epsilon)\cdot Poisson(N, q\,\bar{N}) \qquad (14)$$

where

$$p^{(1)}(k;q,\epsilon) = \frac{1+F_2}{(1+F_1)^2}\left[p_G^{(1)}(k;q,\epsilon) + \frac{1}{qk!}\sum_{j=k}^{\infty}\frac{(-1)^{j-k}}{(j-k)!(2j)^{3/2}}\epsilon^j F_j\right] \qquad (15)$$

According to Chen et al.[18]

$$p_G^{(1)}(k;V_0,\epsilon) = \frac{\pi\omega_0{}^2 z_0}{V_0 k!}\int_0^{\infty}\gamma(k,\epsilon e^{-2x^2})\,dx \qquad (16)$$

where, $\gamma(a, x)$ is the incomplete gamma function. q is the ratio between an ideal Gaussian shaped detection volume defined in FCS, V_{FCS}, and a reference volume, V_0 (i.e., $V_0 = qV_{FCS}$). It is found that the probability distribution $P(k; \bar{N}, \epsilon)$ is independent of the choice of V_0, as long as V_0 is large enough to obtain a positive value of $P(0; \bar{N}, \epsilon)$.[18,24] We found $q = 6$ to be an appropriate choice for our experiment. A first-order correction in which $F_j = F$ for $k = 1$ and $F_j = 0$ for $k > 1$ was used. F is the ratio between out-of-focus and in-focus emission. For our optical setup, F is found to be ~0.7, in good agreement with the PCH measurements of Huang et al. using a similar optical setup.[24] The probability distribution for a two-component system is obtained from the above equations using

$$P(k;\bar{N}_1,\epsilon_1,\bar{N}_2,\epsilon_2) = P(k;\bar{N}_1,\epsilon_1)\otimes P(k;\bar{N}_2,\epsilon_2) \qquad (17)$$

Our PCH measurements could be analyzed by fitting to eq 17. The parameters $\bar{N}_1$, $\bar{N}_2$, ϵ_2, and F were determined, with the parameter ϵ_1 held constant (see Table 1).

An alternative approach to the PCH analysis was to apply a single-species model that depended on an *apparent* number of

molecules, $\bar{N}_{app}$, with an *apparent* specific brightness, ϵ_{app}.[38,39] $\bar{N}_{app}$ and ϵ_{app} are weighted averages characterizing the distribution of fluorescent species of differing brightnesses present in the sample. For a two-component system, these parameters are given by eqs 18 and 19

$$\bar{N}_{app} = \frac{(\bar{N}_1\epsilon_1 + \bar{N}_2\epsilon_2)^2}{\bar{N}_1\epsilon_1^2 + \bar{N}_2\epsilon_2^2} \tag{18}$$

$$\epsilon_{app} = \frac{\bar{N}_1\epsilon_1^2 + \bar{N}_2\epsilon_2^2}{\bar{N}_1\epsilon_1 + \bar{N}_2\epsilon_2} \tag{19}$$

Our PCH data could be analyzed by fitting to the single-component distribution (eq 14) with $\bar{N} = \bar{N}_{app}$ and $\epsilon = \epsilon_{app}$. The parameters $\bar{N}_{app}$, ϵ_{app}, and F were obtained.

Table 1 compares the PCH parameters obtained using the different analysis procedures for a representative set of data. The results were essentially equivalent in that they gave the same values for $\bar{N}_{app}$, ϵ_{app}, and F. They also agreed with the corresponding parameters derived from FCS within experimental error. In particular, we notice that $\bar{N}_{app}$ has the same functional form as the inverse amplitude of the autocorrelation function, $[G_{A,2S}(0) - 1]^{-1}$. Good consistency between these parameters was found for both analysis procedures. The advantage of the two-component PCH analysis is that the equilibrium constant, K_{FFS}, can be determined directly from the PCH data alone. The disadvantage is that four adjustable parameters are needed to fit the data, which means the parameters were not as well determined as one would wish (~20- to 30-% relative standard deviations for $\bar{N}_1$ and $\bar{N}_2$). The single-component analysis requires fewer adjustable parameters, so the parameters were determined more precisely (<10-% relative standard deviations). However, K_{FFS} could not be obtained directly because the one-component PCH analysis did not provide enough information to uniquely determine $\bar{N}_1$ and $\bar{N}_2$. We found the best precision for determining K_{FFS} was attained by combining the information from the one-component PCH with the FCS parameters. Using eqs 13, 18, and 19, along with the known value of ϵ_1, we obtain

$$\bar{N}_1 = \frac{\bar{N}_{app}\epsilon_{app}^2}{[\epsilon_1^2 + (\epsilon_1 - \epsilon_{app})^2/B_{eq}]} \text{ and} \tag{20}$$

$$K_{FFS} = \frac{\bar{N}_{CC} - \bar{N}_1}{\bar{N}_1} \tag{21}$$

Table 1 shows the values of $\bar{N}_1$, $\bar{N}_2$, and K_{FFS} derived from the above equations for a representative sample.

Failure of the Two-State Reaction Mechanism. In the past, it was assumed that the sub-millisecond chemical relaxation processes observed by FCS represented the complete DNA hairpin folding reaction.[7,8,12−15] If this were the case, then K_{melt} and K_{FFS} would be identical. We are now in a position to evaluate that assumption. Figure 3A compares the behavior of K_{melt} and K_{FFS} as a function of NaCl concentration. There is good agreement between the two sets of constants at NaCl concentrations below ~25 mM. At these lower NaCl concentrations, the open form of the DNA hairpin is favored at our laboratory temperature. At higher concentrations, however, the deviation becomes quite dramatic. The melting curves predict a precipitous rise in the equilibrium constant with increasing NaCl concentration as already discussed; whereas, the equilibrium constant determined by PCH and FCS stays relatively constant. According to our observations, the assumption that K_{melt} and K_{FFS} describe the same reaction is only valid under conditions that favor the open form of the hairpin. When the closed form of the hairpin is favored, K_{melt} and K_{FFS} appear to represent different reactions. This is our first clue that the DNA hairpin folding reaction may be more complicated than previously recognized.

Additional clues come from the behavior of the FCS and PCH parameters themselves. Figure 5A shows the behavior of $\bar{N}_{app}$, ϵ_{app}, $[G_A(0) - 1]$ (the autocorrelation amplitude), $\langle I \rangle$ (the average photocount rate), and $\bar{N}_{CC}$ as a function of NaCl concentration. Also shown is the way these parameters would behave assuming a two-state reaction characterized by the equilibrium constant, K_{melt} (dotted curves). The parameters are plotted against $K_{melt}/(K_{melt} + 1)$ for each NaCl concentration, which represents the folded fraction of DNA hairpins that would be present assuming a two-state reaction. The dotted curves were calculated using this predicted fraction, along with the measured values of ϵ_1 and ϵ_2. (See Supporting Information for the details of the calculation.) In a two-state reaction $\bar{N}_{app}$ should slowly decrease to a minimum value, while $[G_{A,2S}(0) - 1]$ should have the inverse of this trend. ϵ_{app} would decrease as the brighter species is depleted in favor of the darker species, and $\bar{N}_{CC}$, which represents the total DNA concentration, should remain constant. What we have observed is diametrically opposed to these expectations. At low NaCl concentrations, all the parameters are in good agreement with their expected values. But as NaCl is added, $\bar{N}_{app}$ drops precipitously, as $[G_A(0) - 1]$ rises inversely. $\bar{N}_{CC}$ abruptly drops, while ϵ_{app} remains relatively constant.

Naturally, we wondered if this apparently anomalous behavior could be due to experimental error or to misinterpretation of our measurements. To address this possibility, we constructed a model two-state system[40] and subjected it to the same set of measurements as described above. The model system consisted of solutions containing poly(dT)$_{40}$ ssDNA, singly labeled with either R6G- or Cy3- and mixed together to achieve different fluorophore ratios. PCH analysis of pure component solutions was used to measure the molecular brightnesses, ϵ_{R6G} and ϵ_{Cy3}. ϵ_{R6G} was identical to ϵ_1, presented above. ϵ_{Cy3} was measured under the same experimental conditions. The ratio $\epsilon_{Cy3}/\epsilon_{R6G}$ was ~0.25 which compares reasonably well to the Q value measured for the DNA hairpins. (See Supporting Information.) Figure 5B shows how $\bar{N}_{app}$, ϵ_{app}, $[G_A(0) - 1]$, $\langle I \rangle$, and $\bar{N}_{Cy3} + \bar{N}_{R6G}$, as determined by FCS and PCH analysis, changed with an increasing fraction of Cy3-labeled ssDNA. The concentrations of the different components were adjusted so that the total DNA concentration remained constant. These parameters behave in precisely the way one would expect for a two-state system. Moreover, the observed trends are completely analogous to the expected behavior of DNA hairpin molecules undergoing a two-

(38) Chen, Y.; Mueller, J. D.; Ruan, Q.; Gratton, E. *Biophys. J.* **2002**, *82*, 133−144.
(39) Chen, Y.; Wei, L.; Mueller, J. D. *Proc. Natl. Acad. Sci. U.S.A.* **2003**, *100*, 15492−15497.
(40) Chen, Y.; Muller, J. D.; Tetin, S. Y.; Tyner, J. D.; Gratton, E. *Biophys. J.* **2000**, *79*, 1074−1084.

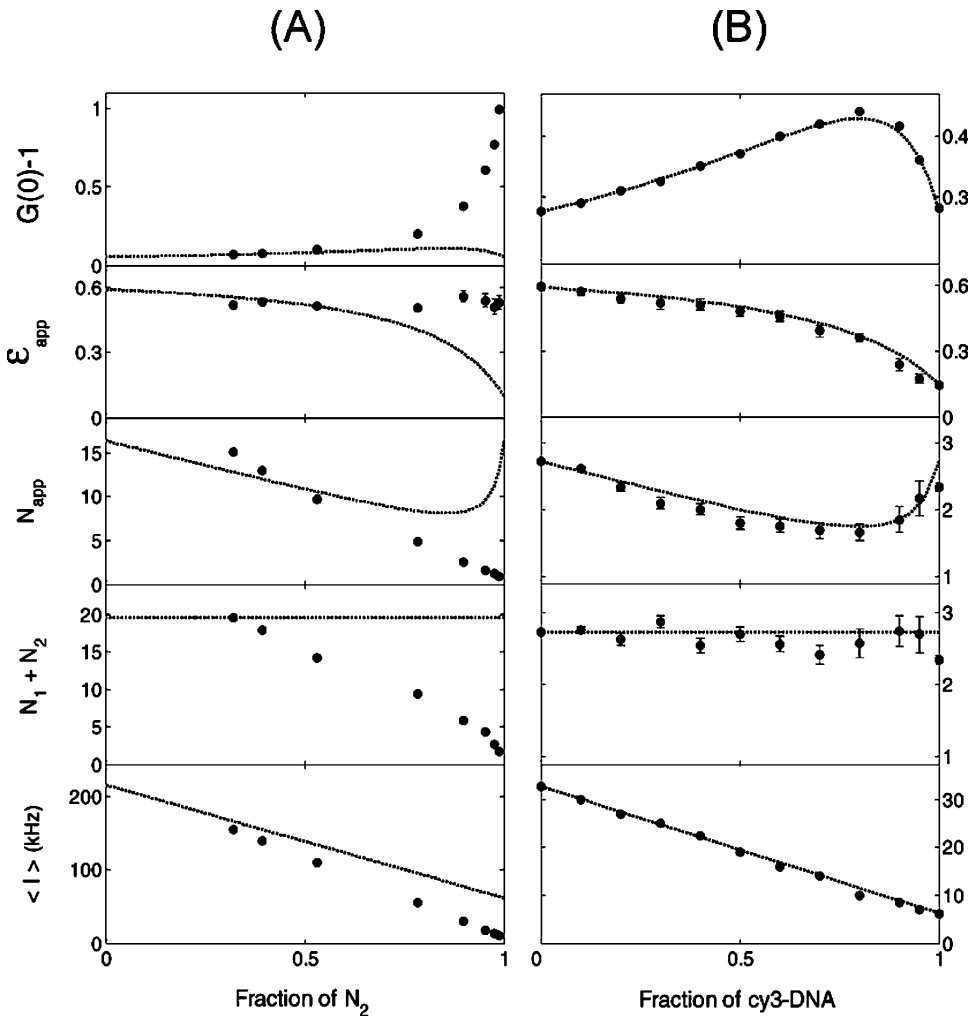

Figure 5. FCS and PCH parameters of DNA hairpin samples (A) and a model two-state system (B). The DNA hairpin samples contained ~25 nM DNA concentrations and varying concentrations of NaCl. The model system contained Cy3- and R6G-singly labeled poly(dT)$_{40}$ single-stranded DNA prepared in different ratios. The total concentration of Cy3 and R6G were held constant at ~4.5 nM. In panel A, the *x*-coordinate represents the expected fraction, $f = K_{melt}/1 + K_{melt}$, of DNA molecules in the folded conformation, assuming a two-state reaction. $\bar{N}_1 + \bar{N}_2$ was obtained from the cross-correlation analysis. In panel B, $\bar{N}_{app}$ and ϵ_{app} were evaluated using fitting parameters from the two-species PCH analysis according to eqs 18 and 19. The expected behaviors of the parameters, assuming a two-state system for each, are represented by dotted lines in both panels (see Supporting Information for details).

state reaction. We conclude that our experiment is capable of characterizing this type of two-state behavior.

We also considered the possibility of detector saturation artifacts skewing the results for higher count rate samples, as well as changes in the background photocount rate due to added NaCl. Detector saturation artifacts were investigated by carrying out the same measurements on samples in which the DNA hairpin concentrations were adjusted to achieve the maximum count rate observed in our experiments for each sample. The same was done for the model two-state system. The model system exhibited precisely the behavior that would be expect for a two-state system, while the DNA hairpin samples exhibited behavior that was anomalous for a two-state system (see Supporting Information). Also, analysis of solvent blanks vs NaCl concentration showed no change in the background photocount rate. Finally, we examined the effect of added NaCl on the fluorescence emission of the R6G fluorophore for both the free fluorophore and the fluorophore labeled DNA hairpin molecule in the absence of quencher. The same was done for 40-oligo polythymine single-stranded DNA labeled at the 3′ and 5′ ends with dabcyl and R6G, respectively. No NaCl concentration dependent effects were observed in any of the samples (see Supporting Information). It is concluded that if the DNA hairpins were reacting according to a two-state mechanism, this would be manifested in the behavior of the FCS and PCH parameters. The fact that the FCS and PCH parameters deviate so strongly from the expected behavior leads us to consider alternative reaction mechanisms for DNA hairpin folding.

Three-State Reaction Mechanism. The observations presented so far can be explained in a straightforward manner if we make the following assumptions. First, it is apparent that the concentration of DNA molecules detectable by PCH and FCS decreases as the DNA hairpin folding reaction progresses. This is evident from the way $\bar{N}_{app}$, ϵ_{app}, $\bar{N}_{CC}$, and the correlation amplitudes are affected by the NaCl concentration, and it suggests that some of the DNA is being converted into a nonfluorescent dark state that does not contribute to the FCS and PCH measurements. Second, it is apparent that this dark state is being formed, and is stable, on a longer time scale than the FCS correlation time. Our FCS experiment can only observe chemical reactions that occur on a faster time scale than the

molecular transport time through the optical detection region. Anything taking place on a longer time scale than ~1 ms is static with respect to FCS. What our results suggest is that the undetectable dark state is static on the FCS time scale and is thus not taking part in the sub-millisecond chemical relaxation process observed by FCS. As far as our FCS and PCH measurements are concerned, this nonfluorescent dark state is a sink into which DNA molecules disappear and never return.

This implies that the DNA hairpin folding reaction is not going to completion on the time scale probed by FCS, as has previously been thought. Some other reaction must be responsible for the observed sub-millisecond relaxation process. How can we be sure this is the case? In fact, *all* our observations point to this key assertion, but it can be explained most clearly with reference to the way the cross-correlation amplitude rises with added NaCl. As already discussed, sub-millisecond chemical relaxation processes observed by FCS do not contribute to the cross-correlation amplitude because they occur too rapidly to remain correlated on the FCCS time scale. Hence, the cross-correlation amplitude is inversely proportional to the *total* concentration of all species taking part in the relaxation. If the observed relaxation represented the complete hairpin folding reaction, then the overall concentration of DNA species involved in the reaction would not change on the FCS time scale. Consequently, the cross-correlation amplitude would remain essentially constant as the reaction progressed (actually, there would be a slight decrease in the amplitude due to the dependence on τ_D). The only way we can explain the dramatic rise in the cross-correlation amplitude with added NaCl is to assume that the sub-millisecond chemical relaxation observed by FCS does *not* represent the complete folding reaction. Rather there must be at least one intermediate step along the way. It is this intermediate reaction that causes the observed chemical relaxation, not the complete folding reaction. As the folding reaction progresses, the DNA species taking part in the observed chemical relaxation are depleted, lowering the total concentration of detectable DNA, raising the cross-correlation and autocorrelation amplitudes, and lowering the apparent number of molecules probed by PCH. At present, we cannot rule out the possibility that the complete reaction may be occurring on a similar time scale to the cross-correlation measurements (~1 ms to ~10 ms) or longer, but it is clearly not occurring any faster than this.

The simplest reaction mechanism that supports our observations is the three-state reaction:

$$\bar{N}_1 \underset{k_{-1}}{\overset{k_1}{\rightleftharpoons}} \bar{N}_2 \underset{k_{-2}}{\overset{k_2}{\rightleftharpoons}} \bar{N}_3 \tag{22}$$

$$K_1 = \frac{\bar{N}_2}{\bar{N}_1}, K_2 = \frac{\bar{N}_3}{\bar{N}_2} \tag{23}$$

$\bar{N}_1$ refers to the unfolded DNA conformation for which the R6G fluorescence is unquenched. $\bar{N}_2$ refers to a reaction intermediate that is stable on the sub-millisecond time scale of the FCS experiment. $\bar{N}_3$ is the fully folded DNA hairpin. We believe the fully folded species represents the proposed dark state in which the R6G fluorescence is efficiently quenched and rendered undetectable by PCH and FCS. The autocorrelation and cross-correlation functions for this three-state reaction mechanism are given by eq 24 (see Supporting Information for a complete derivation):

$$G_{3S}(\tau) - 1 = \frac{1}{\bar{N}_{total}}(1 + B_1 e^{\lambda_2 \tau} + B_2 e^{\lambda_3 \tau}) g_D(\tau) g_T(\tau) g_F(\tau) \tag{24}$$

where $\bar{N}_{total}$ is the total concentration of DNA in all its forms ($\bar{N}_{total} = \bar{N}_1 + \bar{N}_2 + \bar{N}_3$); B_1, B_2, λ_2, and λ_3 are functions of the rate and equilibrium constants; and $g_D(\tau)$, $g_T(\tau)$, and $g_F(\tau)$ are as defined in eqs 6, 7, 9, and 11.

From the previous discussion, it can be assumed that k_1, $k_{-1} \gg k_2$, k_{-2}. Accordingly, the chemical relaxation process observed by our FCS experiment arises from the two-state $\bar{N}_1 \rightleftharpoons \bar{N}_2$ reaction. The $\bar{N}_2 \rightleftharpoons \bar{N}_3$ reaction occurs on a time scale not observable by FCS (i.e., slower than the diffusion and flow time of molecules through the optical probe region). This implies that the DNA molecules fluctuate between open and intermediate configurations many times before the correctly folded stem-loop hairpin structure is formed. Under these conditions, $G_{3S}(\tau)$ takes on approximately the same functional forms as $G_{2S}(\tau)$ in eqs 5 and 8 (see Supporting Information). The key differences are that $\bar{N}_2$ now refers to the reaction intermediate, K_{FFS} refers to K_1, τ_R is the relaxation time of the $\bar{N}_1 \rightleftharpoons \bar{N}_2$ reaction, and ϵ_2 is the specific brightness of R6G in the intermediate state. The equations for $\bar{N}_{app}$ and ϵ_{app} (eqs 18 and 19) are redefined similarly.

All of the observations presented above can now be explained. K_{FFS} and K_{melt} exhibit different dependences on NaCl because K_{FFS} only describes the $\bar{N}_1 \rightleftharpoons \bar{N}_2$ reaction; whereas, K_{melt} describes the complete folding reaction (it should be noted that eq 12 assumes a two-state reaction mechanism, so K_{melt} may not represent the actual equilibrium constant for the complete reaction). At low NaCl concentrations, the $\bar{N}_1 \rightleftharpoons \bar{N}_2$ reaction dominates, so K_{FFS} and K_{melt} are essentially equivalent. As NaCl is added, the $\bar{N}_2 \rightleftharpoons \bar{N}_3$ reaction becomes dominant, such that K_{melt} rises, while K_{FFS} changes more slowly. NaCl apparently does not affect the $\bar{N}_1 \rightleftharpoons \bar{N}_2$ reaction equilibrium as strongly as it does on the complete folding reaction. The behavior of $\bar{N}_{app}$, ϵ_{app}, $[G_A(0) - 1]$, and $\bar{N}_{CC}$ can also be explained. The FCS and PCH measurements are only sensitive to $\bar{N}_1$ and $\bar{N}_2$. At low NaCl concentrations, $\bar{N}_1$ and $\bar{N}_2$ represent the dominant species, so the PCH and FCS parameters behave as expected for a two-state reaction. As the reaction progresses, $\bar{N}_1$and $\bar{N}_2$ are depleted, which causes the observed drop in $\bar{N}_{app}$ and $\bar{N}_{CC}$ and the corresponding rise in the correlation amplitudes. Also, because K_{FFS} changes slowly with added NaCl, the change in the relative concentrations of $\bar{N}_1$ and $\bar{N}_2$ is correspondingly slow, which explains why ϵ_{app} is not affected by the addition of NaCl.

This three-state reaction can be quantified in the following way. At 0 M NaCl, it is assumed that only $\bar{N}_1$ and $\bar{N}_2$ are appreciable.[37] Hence, the total amount of DNA for all the samples is approximately $\bar{N}_{total} = \bar{N}_1$ (0 M NaCl) + $\bar{N}_2$ (0 M NaCl), which is measured by FCS and PCH. The same procedure can then be used to measure $\bar{N}_1$ (x M NaCl) and $\bar{N}_2$ (x M NaCl) for all subsequent samples. $\bar{N}_3$ (x M NaCl) is obtained for each sample using $\bar{N}_3 = \bar{N}_{total} - (\bar{N}_1 + \bar{N}_2)$. Figure 6 shows the results of these measurements.

Our analysis can also explain the observed melting curves. We define a parameter $K_{melt,3S}$ that can be calculated for each

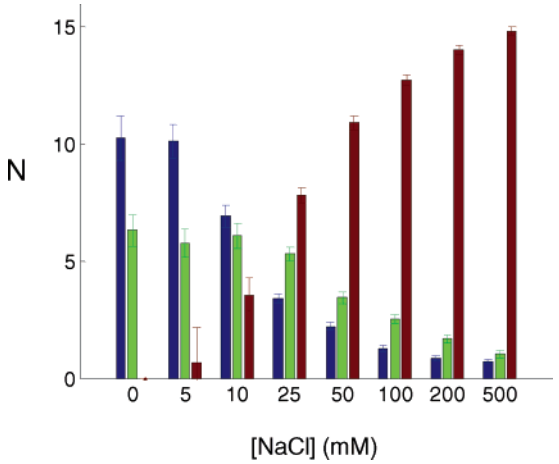

Figure 6. Equilibrium distribution of the three DNA hairpin conformations ($\bar{N}_1$) blue, ($\bar{N}_2$) green, ($\bar{N}_3$) red) determined by the three-state reaction mechanism. The unfolded and intermediate forms of the DNA hairpin are favored at low NaCl concentration, while the folded form is favored at high NaCl concentration.

sample using data from our FCS and PCH analysis for comparison with the K_{melt} values obtained directly from the melting curves. By analogy to eq 12, we have

$$K_{melt,3S,i} = \frac{\langle I\rangle_{max} - \langle I\rangle_i}{\langle I\rangle_i - \langle I\rangle_{min}} \tag{25}$$

where $\langle I\rangle_i$ is the average fluorescence count rate observed in our FCS and PCH experiment for a given NaCl concentration. $\langle I\rangle_{max}$ and $\langle I\rangle_{min}$ are the fluorescence count rates that would be observed from samples in which all the DNA was present in a completely open or a completely closed form, respectively. (See Supporting Information for the details of calculation.) As seen in Figure 3A, the $K_{melt,3S}$ and K_{melt} values are in remarkably good agreement.

Discussion. Previous studies on DNA hairpin formation have assumed a folding free energy landscape comprising two potential minima, corresponding to the random coil and the fully folded stem-loop hairpin, and a transition state ensemble of partially folded or misfolded intermediates.[6−9,11−16] These intermediate states cause roughness of the free energy surface but are short-lived on the time scale of the folding reaction. Recent atomistic molecular dynamics simulations identified some plausible intermediate structures in the unfolding of a small hairpin forming RNA molecule that may be present in the transition state ensemble.[41,42] These simulations, together with a statistical mechanics model developed by Ansari et al.,[6,9,11] suggest a heterogeneous transition state ensemble consisting of collapsed hairpinlike structures in which the loop is fully or partially formed and the stem is held together by single native or nonnative base-pair contacts.

Our observations suggest the DNA hairpin folding picture may need to be expanded to accommodate longer-lived reaction intermediates that do not lead directly to the completely folded stem-loop hairpin structure. Candidates for such species can also be found in the molecular dynamics simulations of Sorin et al.[41,42] The majority of the folding trajectories observed by these authors terminated in "collapsed" structures containing nativelike hairpin loops, but with stem structures that were misfolded in a variety of ways. This "collapsed ensemble" was distinct from the transition state ensemble in that a much longer reaction time (~8 μs) for forming the collapsed structures was observed, indicating a higher stability of these structures compared to those of the transition state.

We propose that the DNA folding reaction being probed by our FCS experiment corresponds to the formation of a collapsed ensemble of long-lived intermediates analogous to the ones observed in the molecular dynamics simulations of Sorin et al.[41,42] This seems consistent with the observations that the simulated collapse occurred on the same time scale as the experimentally observed reaction time for hairpin folding and that most of the simulated folding reactions resulted in these types of misfolded structures. It may explain why we observed a finite value of ϵ_2 in our PCH measurements. Misfolding of the stem sequence may give rise to partial or intermittent contact between the R6G fluorophore and the dabcyl quencher, thereby lowering the quenching efficiency. The formation of the completely folded stem structure occurs on a time scale that is too slow to be observed by FCS. Yet once formed, this structure is highly stable on the FCS time scale. This, too, is consistent with the molecular dynamics simulations of Sorin et al.,[41,42] who found that spontaneous unfolding of a fully formed stem-loop hairpin was an extremely rare event.

Experimental support for the proposed mechanism comes from single-pair Förster resonance energy transfer (FRET) experiments on donor−acceptor labeled DNA hairpins by Grunwell et al.[43] and forced unzipping experiments of RNA hairpins by Liphardt et al.[44] and Cocco et al.[45] These authors observed much longer folding and unfolding reaction times than would be predicted from solution phase kinetics experiments on the same sized hairpins. One can argue that these experiments were carried out under somewhat extreme conditions and may not represent the true behavior of DNA hairpins in free solution. However, an alternative assumption is that these experiments were probing a different aspect of the folding reaction. Whereas the solution phase kinetics experiments probed the intermediate $\bar{N}_1 \rightleftharpoons \bar{N}_2$ reaction, the single-pair FRET and forced unzipping experiments may have been probing the complete folding reaction. This may explain why such vastly different time scales were observed.

How do our observations impact the conclusions drawn from previous kinetics experiments regarding the energetics of DNA hairpin loop formation? On one hand, the reactions being probed are still thought to be loop-forming reactions and are therefore valid models from which to gain insight into DNA hairpin loop formation. However, many of the conclusions drawn from previous experiments are based on the temperature and loop size dependence of the rate constants for hairpin loop formation (k_1 in eq 4). These constants were calculated using the measured reaction times, combined with equilibrium constants derived from analysis of the melting curves. We have shown that when conditions favor the closed form of the hairpin, the equilibrium

(41) Sorin, E. J.; Rhee, Y. M.; Nakatani, B. J.; Pande, V. S. *Biophys. J.* **2003**, *85*, 790−803.
(42) Sorin, E. J.; Rhee, Y. M.; Pande, V. S. *Biophys. J.* **2005**, *88*, 2516−2524.
(43) Grunwell, J. R.; Glass, J. L.; Lacoste, T. D.; Deniz, A. A.; Chemla, D. S.; Schultz, P. G. *J. Am. Chem.* Soc. **2001**, *123*, 4295−4303.
(44) Liphardt, J.; Onoa, B.; Smith, S. B.; Tinoco, I.; Bustamante, C. *Science* **2001**, *292*, 733−737.
(45) Cocco, S.; Marko, J. F.; Monasson, R. *Eur. Phys. J. E* **2003**, *10*, 153−161.

constant derived from the melting curve does not describe the reaction being probed by the kinetics experiment. Hence, rate constants determined in this way may be in error. Just how severe might these errors be? For our DNA hairpin sample under conditions of 100 mM NaCl, we obtain $k_1 = (1.12 \pm 0.16) \times 10^4\ s^{-1}$, based on our τ_R and K_{FFS} measurements for this sample. If we use K_{melt} in our calculation, we obtain $k_1 = (1.53 \pm 0.21) \times 10^4\ s^{-1}$. Although the use of K_{melt} may overestimate the rate constant somewhat, k_1 does not have a strong dependence on the equilibrium constant when $K > 1$. When $K < 1$, the reactions probed by the kinetics experiments are the same as the ones described by the melting curves. Hence, we believe conclusions drawn from the behavior of k_1 can still be supported.

However, conclusions regarding the reverse reaction are a different matter, because the k_{-1} rate constant depends much more strongly on the reaction equilibrium when $K > 1$. For example, our 100 mM NaCl sample gives $k_{-1} = (4.79 \pm 0.50) \times 10^3\ s^{-1}$ and $k_{-1} = (6.46 \pm 0.74) \times 10^2\ s^{-1}$ using K_{FFS} and K_{melt}, respectively. One area of controversy in the literature on the unfolding of DNA hairpins has to do with the loop size dependence of k_{-1}. Some studies have found that k_{-1} has no dependence on loop size.[8] Others show an increase in k_{-1} with loop size, and still others show a decrease.[11,15] We believe these conflicts come from the fact that some experiments were carried out under conditions that favored the closed form of the hairpin, while others were carried out under conditions in which the open form was favored. Conclusions drawn from the k_{-1} parameter are only valid when conditions favor the open form. Even then, we believe the reaction described by k_{-1} pertains to the dissociation of a misfolded stem structure, not the unwinding of a fully intact set of base pairs.

Conclusions

We have shown that more detailed information about the DNA hairpin folding reaction can be obtained by combining fluorescence autocorrelation and cross-correlation measurements with PCH analysis. These measurements support a three-state reaction mechanism for DNA hairpin formation that consists of a rapid equilibrium between open and intermediate forms of the DNA and a fully folded form that is stable on the time scale of our FCS experiment. Further insight into this proposed mechanism could be gained by carrying out these measurements on DNA hairpins with varying stem and loop sizes and compositions. For example, a smaller sized hairpin with a shorter stem sequence may exhibit folding times for both the intermediate reaction and the final folding reaction that could be measured on the FCS time scale simultaneously. Also, it is suggested that the experimental techniques described in this paper could be employed in the future to the study of more complicated biomolecule folding reactions involving RNA, DNA aptamers, proteins, and protein−nucleic acid complexes.

Acknowledgment. This research was supported by the National Institutes of Health-National Center for Research Resources (Grant Number RR017025). We thank Richard N. Zare and Thomas D. Perroud for assisting us with the PCH analysis of our data, Ming Yu for technical assistance, and Markus Sauer for helpful discussions.

Note Added after ASAP Publication. A correction was made to the reaction notation in the fourth sentence of the second full paragraph after eq 24, after the initial ASAP publication on January 5, 2006.

Supporting Information Available: Derivation of three-state FCS model; Further details on the analysis of the PCH and FCS data ((i) Combined approach with FCS and PCH analysis, (ii) PCH analysis of model two-state system, (iii) PCH analysis of DNA hairpin sample, (iv) Calculation of expected behavior of parameters, (v) FFS experiments with varying sample concentration, and (vi) Calculation of $K_{melt,3S}$); Control experiments to determine the effect of NaCl on the R6G fluorescence. This material is available free of charge via the Internet at http://pubs.acs.org.

JA0560736